

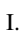


# Algorithmic Integration and Quantification of Endoscopic and 3D TEE Images in Mitral Valve Surgery

M. Ivantsits<sup>1,2</sup> , M. Huellebrand<sup>1,2,3</sup>, L. Walczak<sup>1,2,3</sup> , J. Welz<sup>5</sup>, D. Greve<sup>2</sup>, I. Wamala<sup>2</sup>, S. Suendermann<sup>2,4</sup>, J. Kempfert<sup>2,4</sup>, V. Falk<sup>2,4</sup>, and A. Hennemuth<sup>1,2,3,4</sup> 

<sup>1</sup>Institute for Imaging Science and Computational Modelling in Cardiovascular Medicine, Charité – Universitätsmedizin Berlin, 13353 Berlin, Germany

<sup>2</sup>Deutsches Herzzentrum der Charité, 13353 Berlin, Germany

<sup>3</sup>Fraunhofer MEVIS, Max-von-Laue-Str. 2, 28359 Bremen, Germany

<sup>4</sup>DZHK (German Centre for Cardiovascular Research), 10785 Berlin, Germany

<sup>5</sup>TNG Technology Consulting GmbH, 85774 Unterföhring, Germany

## Abstract

Minimally invasive surgery is the state-of-the-art approach for repairing the mitral valve, which controls the blood flow into the left heart chamber. The surgeons rely on camera and sensor technologies to support visualization, navigation, and measurement. As patients are connected to the cardio-pulmonary bypass, the anatomy is severely deformed by the altered pressure conditions. We developed a technique that combines stereo-endoscopic video with three-dimensional transesophageal echocardiography (3D TEE) to improve anatomic visualization and measurement accuracy during mitral valve repairs. Our methodology includes stereo camera calibration, image segmentation, and 3D model reconstruction. Anatomical landmarks are used to align the imaging modalities. This approach allows the visualization of pre-operatively determined mitral valve properties, e.g., overlaying heat maps in stereo endoscopic data. Our validation results showed high precision and accuracy within an error range of  $0.5 \pm 0.1$  mm. The effectiveness of the heatmap visualization in complex prolapse cases varied. Integrating stereoscopic and 3D TEE promises greater precision in mitral valve repairs. In the future, this approach can also be used to visualize local tissue properties or the optimal locations of implants.

## CCS Concepts

• **Computing methodologies** → **Image segmentation; Matching; Reconstruction; Interest point and salient region detections; Shape inference;**

## 1. Introduction

The mitral valve is located between the left atrium and left ventricle (see Figure 1 A). It functions as a one-way valve, ensuring unidirectional blood flow from the atrium to the ventricle during the cardiac cycle. Comprising two leaflets, the mitral valve opens to allow blood to flow into the left ventricle in diastole and closes to prevent backflow into the atrium in systole. Proper mitral valve functioning is essential for maintaining efficient cardiac output. Mitral regurgitation (MR) is a common pathology of the mitral valve, characterized by the valve's inability to close properly, leading to backward blood flow into the left atrium during systole. Surgical repair is the primary treatment for MR [GWB\*01]. Its success heavily depends on an accurate anatomical and functional understanding of the mitral valve. Traditional open-heart surgery, while effective, is associated with extended recovery periods. Minimally invasive techniques have emerged as a promising alternative, offering reduced patient trauma and faster recovery [SCF15]. Among these advancements, integrating stereo-endoscopic measurements with pre-surgical three-dimensional

(3D) transesophageal echocardiography (TEE) data represents a step forward in the precision and efficacy of mitral valve repair. Figure 1 A illustrates a typical setup during minimally invasive mitral valve repair, which is necessary during surgery.

Existing fusion methods primarily focus on preoperative planning and visualization, often involving rigid transformations suitable for regions with minimal motion, such as ear, nose, and throat (ENT) [LSB\*19, DGS\*02, IYB\*17, BLI\*05]. Other methods focus on the fusion of abdominal structures [AHR13, BNA\*16, KYCJ\*] or cardiac structures [SWGPO5]. The literature exhibits methods fusing endoscopic images with CT [BNA\*16, LSB\*19, IYB\*17, BLI\*05, KYCJ\*, SWGPO5], MRI [AHR13, DGS\*02, SWGPO5], or ultrasound (US) [YWA\*15]. These methods either process the endoscopic images as 2D [BNA\*16, LSB\*19, DGS\*02, IYB\*17], or reconstruct the endoscopic information in 3D by structured light [AHR13] or structure from motion [BLI\*05, KYCJ\*, YWA\*15]. Some methods require the utilization of a C-arm fluoroscope [BNA\*16, LSB\*19] or the invasive placement of markers [DGS\*02] to track the endoscope's position accurately. However, these approaches face challenges

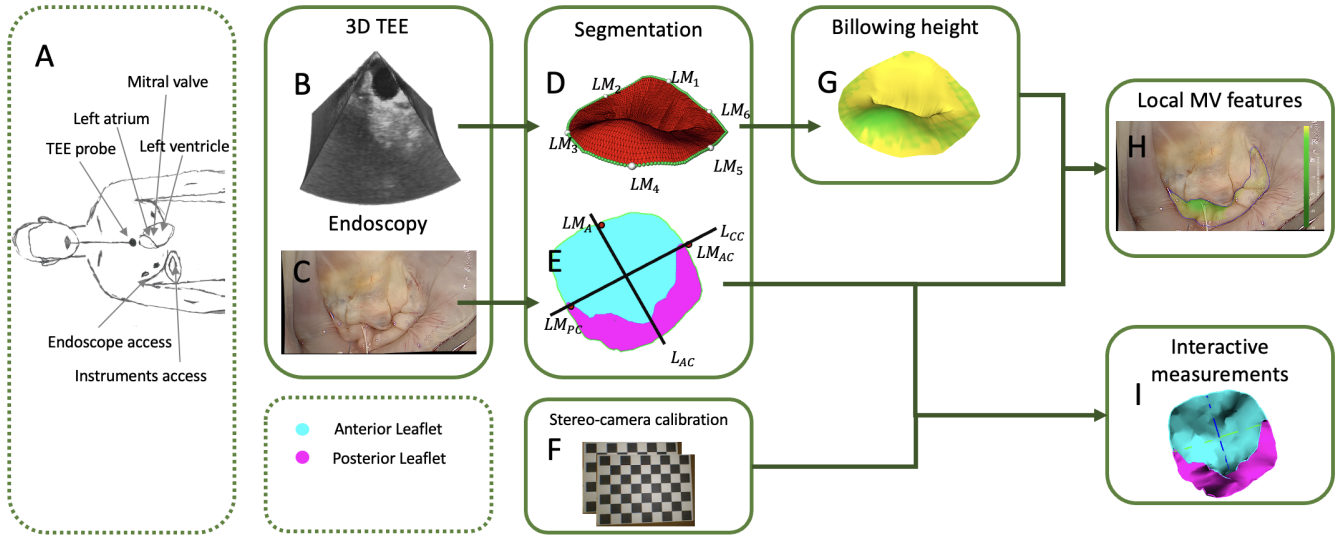


**Figure 1:** Proposed workflow: In 3D TEE images (B) and endoscopic scenes (C) MV and landmarks are detected (D+E). 3D alignment of the MV enables the overlay (H) of parameter heatmaps (G). E illustrates the landmark extraction from an endoscopic segmentation.  $LM_{AC}$  and  $LM_{PC}$  mark the changeover between the leaflets. The upper intersection of the valve annulus and orthogonal line  $L_{AC}$  is denoted as the final landmark  $LM_A$ . Reconstructing the mitral valve as a 3D object (I) in world coordinates enables precise length and area measurements in the endoscopic data.

in cardiac surgery due to the heart's significant deformation after decoupling from circulation.

Common procedures involve acquiring 3D TEE images before cardiopulmonary bypass and using live video endoscopy for visualization. The different states of the heart during these procedures (active beating heart vs. arrested open heart during surgery) and the disparate display formats necessitate mental fusion by the surgeon, complicating the assessment of valve failure mechanisms.

To address these challenges, we propose an algorithmic solution for intra-operative registration of stereo-endoscopic and 3D TEE images without manual input. This method extracts anatomical landmarks and unifies image-based information into a single coordinate system to provide functional and quantitative information during valve repair.

## 2. Dataset

The stereo endoscope image data was recorded with the Einstein-Vision 2.0 Aesculap system. We acquired the data as a video with a spatial resolution of 1920x1080 pixels and a temporal resolution of 30 frames per second. The Aesculap system yields the two channels of the stereo image interlaced by line, giving us the left channel in the odd rows and the right channel in the even ones. The 3D ultrasound image data is acquired with a transesophageal transducer (TEE) with a GE Vingmed Vivid E9 machine.

## 3. Method

**Stereo-camera calibration:** As an initial step, we calibrate the stereo-endoscopic camera. This includes undistortion of the images

and rectification of the stereo pair. We follow the standard approach utilizing a checkerboard as described by [PD96, HZ04]. This process yields intrinsic parameters for each camera, as well as a matrix

$$Q = \begin{bmatrix} 1 & 0 & 0 & -c_x \\ 0 & 1 & 0 & -c_y \\ 0 & 0 & 0 & f \\ 0 & 0 & -\frac{1}{T_x} & 0 \end{bmatrix}, \quad (1)$$

which projects vectors from a disparity map into 3D world coordinates.  $c_x$  and  $c_y$  are the coordinates of the principal point in the left camera,  $f$  is the focal length, and  $T_x$  is the baseline length.

**Endoscopic mitral valve segmentation** The following steps use the U-Net-based segmentation of the endoscopic images, including the anterior and posterior leaflets and the surgical instruments in that scene [ITS\*20].

**Endoscopic landmark extraction** We perform a morphological closing operation to remove holes in the leaflet masks and extract points on the mask's boundary as a contour, denoted as  $C_E$  (highlighted in green in Figure 1 E). Additionally, we extract contours for the anterior leaflet  $C_{EA}$  and posterior leaflet  $C_{EP}$ . The landmarks  $LM_{AC}$  and  $LM_{PC}$  mark the anterolateral and posteromedial commissures at the anterior-to-posterior leaflet transition. We fit a line  $L_{CC}$  through these points (see Figure 1 E). Orthogonal to  $L_{CC}$ , we intersect another line  $L_{AC}$  at the center of  $LM_{AC}$  and  $LM_{PC}$ . The point  $LM_A$  is defined as the upper intersection of contour  $C_E$  and the line  $L_{AC}$ .

**Endoscopic 3D mitral valve model** Based on the undistorted and rectified stereo pair, we calculate the disparity map via semi-global

matching and mutual information as proposed by [Hir08]. We apply the method proposed by [MCL\*14], which calculates the disparity from left to right and right to left and calculates a confidence map of the measured disparities. These confidence values range from 0-255. We remove values that have zero confidence and keep the rest. In conjunction with the segmentation mask described in section 3 and the matrix  $Q$ , we reconstruct the mitral valve anterior  $MV_{EA}$  and posterior  $MV_{EP}$  leaflets as point clouds in 3D world coordinates. We reconstruct the anterior and posterior contours in 3D by projecting the contours  $C_{EA}$  and  $C_{EP}$  using the matrix  $Q$ . Using these separated point clouds and anterior and posterior leaflet contours, we apply the triangulation method described by [IPH\*] to create two surface meshes.

### 3D TEE mitral valve segmentation and landmark extraction

The corresponding mesh-based segmentation of the mitral valve, labeled vertices for the annulus, and a vertex on the annulus closest to the aorta are calculated using the method [IPH\*] (see Figure 1 D). To extract landmarks for registration with endoscopic images, we calculate the center  $LM_A C$  between  $LM_5$  and  $LM_6$  located on the annulus. We further define  $LM_P C$  similarly between  $LM_2$  and  $LM_3$ .  $LM_1$  is defined as  $LM_A$ .

**Billowing height** We utilize the surface mesh and annulus provided by the 3D TEE segmentation to calculate the billowing height (see Figure 1 G). This is done by approximating a minimal surface to the annulus (see Figure 2). After fitting this surface, we calculate the signed distance for each vertex of the mitral valve model to this surface.

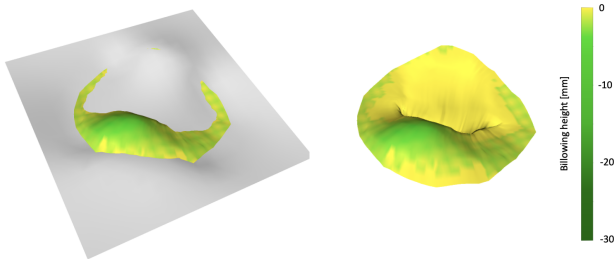


**Figure 2:** The surface fitted through the mitral valve annulus (left) is used to calculate the directed distance for each vertex of the mitral valve surface model (right).

**Landmark-based registration** Three landmarks extracted from the 3D TEE (see 3) are represented as column matrix  $V$  and three landmarks extracted from the endoscopic view (see 3) are also represented as column matrix  $W$ . We calculate  $R_{init}$  and  $t_{init}$ .  $R_{init}$  represents a scaling and rotation matrix and  $t_{init}$  a translation vector. We solve for a linear equation satisfying  $R_{init} \cdot x + t_{init} = y$ . Since we are dealing with three points in each coordinate frame, we can directly derive these parameters (see equations 2, 3, and 4).

$$\begin{aligned} \vec{v}_3 &= \vec{v}_0 + (\vec{v}_1 - \vec{v}_0) \times (\vec{v}_2 - \vec{v}_0) \\ \tilde{V} &= [(\vec{v}_1 - \vec{v}_0) \quad (\vec{v}_2 - \vec{v}_0) \quad (\vec{v}_3 - \vec{v}_0)] \end{aligned} \quad (2)$$

$$\begin{aligned} \vec{w}_3 &= \vec{w}_0 + (\vec{w}_1 - \vec{w}_0) \times (\vec{w}_2 - \vec{w}_0) \\ \tilde{W} &= [(\vec{w}_1 - \vec{w}_0) \quad (\vec{w}_2 - \vec{w}_0) \quad (\vec{w}_3 - \vec{w}_0)] \end{aligned} \quad (3)$$

$$\begin{aligned} R_{init} &= \tilde{W} \cdot \tilde{V}^{-1} \\ t_{init} &= w_0 - R_{init} \cdot v_0 \end{aligned} \quad (4)$$

These parameters initialize the registration of the annulus extracted from the 3D TEE and the endoscopic view, having a correct rotation. We introduce an iterative closest point (ICP) algorithm [AHB87], refining the initial fusion parameters. First, we transform the original points on the contour of the 2D endoscope with the previously acquired parameters. Further, we apply the ICP algorithm on the point cloud  $Y$  and  $X_{init}$ , resulting in the parameters  $R_{icp}$  and  $t_{icp}$ .

**Billowing height heatmap overlay** Following the calculation of the billowing height delineated in section 3 and the subsequent transformation of the three-dimensional Transesophageal Echocardiography (TEE) mitral valve surface into the endoscopic coordinate frame, as explicated in section 3, this study renders the spatial variation in billowing height as a heatmap. This heatmap is then superimposed onto the endoscopic imagery. For each pixel within the endoscopic scene, rays are projected, and intersections with the transformed 3D TEE mitral valve model are detected. The intersecting positions are used to interpolate the respective billowing heights, then recorded within a single-channel image format. The visualization of billowing height employs Red-Green-Blue-Alpha (RGBA) color lookup tables, overlaying the heatmap directly onto the endoscopic images. A diverging colormap, transitioning from red to blue, is utilized to represent both positive and negative billowing heights, a standard in mitral valve visualization techniques. Additionally, a linear colormap ranging from green to yellow is exclusively used for depicting negative billowing heights, hypothesizing that it enhances visibility due to its higher contrast and reduced information saturation in areas of positive billowing heights.

## 4. Results

Experiments were performed on an Intel(R) Core(TM) i7-8700K CPU @ 3.70GHz with 16 GBs RAM and an Nvidia RTX 2080 Ti GPU with 11 GB memory.

### 4.1. Ruler-based measurements validation

We employed a ruler within the atrium to validate our measurement and 3D reconstruction technique during the stereo-endoscopic mitral valve repair procedure. This allowed us to draw splines onto the ruler in a 2D view (see Figure 3), which were then used to reconstruct the 3D scene and measure the path length accurately. This was done by sampling pixels from the disparity map under the drawn spline, followed by a projection into 3D world coordinates with the matrix  $Q$ . This path is integrated to measure the distance.

We conducted these validation experiments on three patients. We performed 10 through-plane and 9 in-plane measurements (relative to the image plane). Additionally, for several experiments, the ruler

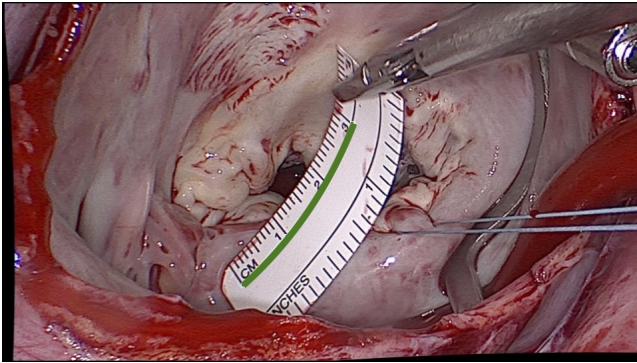


**Figure 3:** An example endoscopic image with a slightly bent ruler held into the scene. The green spline contour illustrates the measured path for this ruler-based validation.

was bent. Figure 4 shows an overview of the errors. The in-plane measurements yielded an error of  $0.5 \pm 0.1$  mm, while the through-plane measurements showed an error of  $0.4 \pm 0.1$  mm.

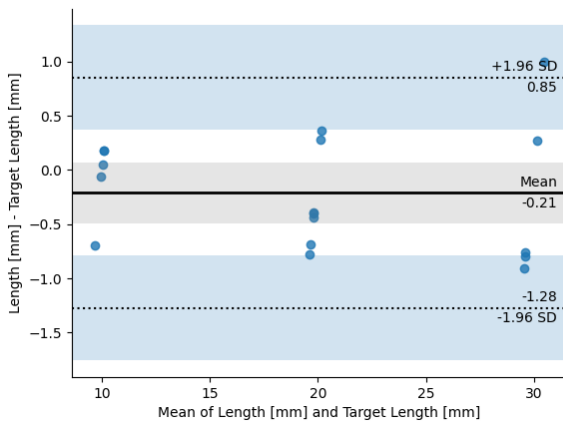


**Figure 4:** Bland-Altman analysis of the length measurement in the stereo-endoscopic images versus the length presented by the ruler.

#### 4.2. Billowing height heatmap overlay

We chose the 3D TEE timepoint for both patients in a fully closed mitral valve configuration to evaluate the billowing height overlay. The endoscopic images were chosen during a mitral valve leakage test. Based on this input, we extracted the valve models and registered them using the method described.

Figure 5 depicts two patients with mitral valve prolapse. The first two images illustrate orthogonal views of the mitral valve in 3D TEE, including the geometry of the mitral valve. The following images illustrate the mitral valve in the endoscopic scene with two alternative heatmap overlay color configurations. The first patient depicts a patient prolapsed on the posterior leaflet (P1, P2). The

second row illustrates a patient with a bi-leaflet prolapse.

The feedback from three clinical experts highlighted that for the first case, where a posterior leaflet prolapse was presented, the heatmap effectively identified the prolapsing region, validating the potential of our approach for precise surgical guidance. However, the heatmap was less useful in the second case, which involved a more complex bi-leaflet prolapse. This underscores the need for further refinement in our approach when dealing with multiple prolapsing segments, where the overlapping regions might dilute the clarity of the heatmap visualization.

Additionally, the feedback on the colormap selection indicated a preference for the green colormap due to its better visibility. However, it was suggested that increasing the contrast could further enhance the utility of the heatmap by making the distinctions between different severity levels more discernible.

#### 5. Discussion

Our results demonstrate a promising integration of stereo-endoscopic imagery with 3D transesophageal echocardiography (TEE), aiming to enhance the precision of mitral valve surgeries. The validation of our measurement techniques through ruler-based validation indicated a high degree of accuracy with in-plane and through-plane measurements, showing an error margin of only  $0.5 \pm 0.1$  mm and  $0.4 \pm 0.1$  mm, respectively. These results suggest that our method can reliably replicate physical measurements within a complex surgical environment and may aid surgical repair during minimally invasive procedures.

However, the deployment of billowing height heatmaps has revealed limitations, particularly in scenarios involving complex anatomical variations such as bi-leaflet prolapse. While effective in cases with simpler pathology, like posterior leaflet prolapse, the overlapping segments in more complex cases reduce the clarity and utility of the visualizations. This suggests the need for refined visualization algorithms to manage anatomical complexities better. Feedback on the color maps used for visualization emphasizes the necessity for iterative improvements to enhance heatmap utility. Clinical experts preferred the green colormap for its visibility but recommended increasing contrast to more clearly differentiate the severity levels of valve prolapse.

#### References

- [AHB87] ARUN K. S., HUANG T. S., BLOSTEIN S. D.: Least-squares fitting of two 3-d point sets. *IEEE Transactions on Pattern Analysis and Machine Intelligence PAMI-9*, 5 (1987), 698–700. 3
- [AHR13] ABDALBARI A., HUANG X., REN J.: Endoscopy-mr image fusion for image guided procedures. *International Journal of Biomedical Imaging 2013* (2013). 1
- [BLI\*05] BURSCHKA D., LI M., ISHII M., TAYLOR R. H., HAGER G. D.: Scale-invariant registration of monocular endoscopic images to ct-scans for sinus surgery. *Med Image Anal 9*, 5 (2005), 413–26. Burschka, Darius Li, Ming Ishii, Masaru Taylor, Russell H Hager, Gregory D Evaluation Study Journal Article Research Support, U.S. Gov't, Non-P.H.S. Netherlands 2005/07/13 Med Image Anal. 2005 Oct;9(5):413-26. doi: 10.1016/j.media.2005.05.005. 1

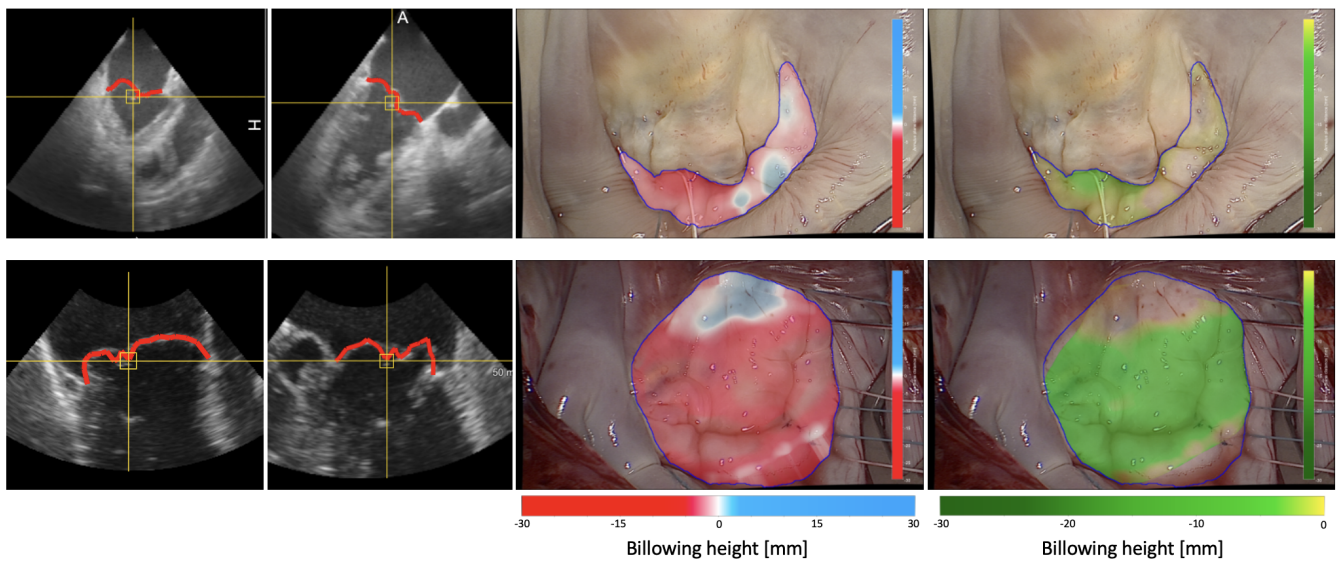


**Figure 5:** An overview of two patients. The first row depicts a patient prolapsed on the posterior leaflet (P1, P2). The second row illustrates a patient with a bi-leaflet prolapse. The first two images are 3D TEE orthogonal slices with annotations of the mitral valve. The next two images show the mitral valve in the endoscopic scene with two alternative heatmap overlay color configurations.

- [BNA\*16] BERNHARDT S., NICOLAU S., AGNUS V., SOLER L., DOIGNON C., MARESCAUX J.: Automatic localization of endoscope in intraoperative ct image: A simple approach to augmented reality guidance in laparoscopic surgery. *Medical image analysis* 30 (2016), 130–143. 1
- [DGS\*02] DEY D., GOBBI D. G., SLOMKA P. J., SURRY K. J. M., PETERS T. M.: Automatic fusion of freehand endoscopic brain images to three-dimensional surfaces: creating stereoscopic panoramas. *IEEE Transactions on Medical Imaging* 21, 1 (2002), 23–30. 1
- [GWB\*01] GILLINOV A. M., WIERUP P. N., BLACKSTONE E. H., BISHAY E. S., COSGROVE D. M., WHITE J., LYTLE B. W., MCCARTHY P. M.: Is repair preferable to replacement for ischemic mitral regurgitation? *J Thorac Cardiovasc Surg* 122, 6 (2001), 1125–41. Gillinov, A M Wierup, P N Blackstone, E H Bishay, E S Cosgrove, D M White, J Lytle, B W McCarthy, P M Comparative Study Journal Article United States 2001/12/01 *J Thorac Cardiovasc Surg*. 2001 Dec;122(6):1125-41. doi: 10.1067/mtc.2001.116557. 1
- [Hir08] HIRSCHMULLER H.: Stereo processing by semiglobal matching and mutual information. *IEEE Transactions on Pattern Analysis and Machine Intelligence* 30, 2 (2008), 328–341. 3
- [HZ04] HARTLEY R., ZISSERMAN A.: *Multiple View Geometry in Computer Vision*, 2 ed. Cambridge University Press, Cambridge, 2004. 2
- [IPH\*] IVANTSITS M., PFAHRINGER B., HUELLEBRAND M., WALCZAK L., TAUTZ L., NEMCHYNA O., AKANSEL S., KEMPFERT J., SÜNDERMANN S., HENNEMUTH A.: 3d mitral valve surface reconstruction from 3d tee via graph neural networks. In *Statistical Atlases and Computational Models of the Heart. Regular and CMRxMotion Challenge Papers*, Camara O., Puyol-Antón E., Qin C., Sermesant M., Suinesiaputra A., Wang S., Young A., (Eds.), Springer Nature Switzerland, pp. 330–339. 3
- [IYB\*20] IVANTSITS M., TAUTZ L., SÜNDERMANN S., WAMALA I., KEMPFERT J., KUEHNE T., FALK V., HENNEMUTH A.: DL-based segmentation of endoscopic scenes for mitral valve repair. 2
- [IYB\*17] INGRAM W. S., YANG J., BEADLE B. M., WENDT R. R., RAO A., WANG X. A., COURT L. E.: The feasibility of endoscopy-ct image registration in the head and neck without prospective endoscope tracking. *PLoS One* 12, 5 (2017), e0177886. 1932-6203 Ingram, W Scott Orcid: 0000-0001-5123-9140 Yang, Jinzhong Beadle, Beth M Wendt, Richard 3rd Rao, Arvind Wang, Xin A Court, Laurence E Journal Article United States 2017/05/26 *PLoS One*. 2017 May 18;12(5):e0177886. doi: 10.1371/journal.pone.0177886. eCollection 2017. 1
- [KYCJ\*] KUMAR A., YEN-YU W., CHING-JEN W., KAI-CHE L., HURNG-SHENG W.: Stereoscopic laparoscopy using depth information from 3d model. In *2014 IEEE International Symposium on Bioelectronics and Bioinformatics (IEEE ISBB 2014)*, pp. 1–4. 1
- [LSB\*19] LAI M., SHAN C., BABIC D., HOMAN R., ELMI TERANDER A., EDSTROM E., PERSSON O., BURSTROM G., DE WIT P. H.: *Image fusion on the endoscopic view for endo-nasal skull-base surgery*, vol. 10951 of *SPIE Medical Imaging*. SPIE, 2019. 1
- [MCL\*14] MIN D., CHOI S., LU J., HAM B., SOHN K., DO M. N.: Fast global image smoothing based on weighted least squares. *IEEE Transactions on Image Processing* 23, 12 (2014), 5638–5653. 3
- [PD96] PAPADIMITRIOU D. V., DENNIS T. J.: Epipolar line estimation and rectification for stereo image pairs. *IEEE Transactions on Image Processing* 5, 4 (1996), 672–676. 2
- [SCF15] SÜNDERMANN S. H., CZERNY M., FALK V.: Open vs. minimally invasive mitral valve surgery: Surgical technique, indications and results. *Cardiovasc Eng Technol* 6, 2 (2015), 160–6. 1869-4098 Sündermann, Simon H Czerny, Martin Falk, Volkmar Comparative Study Journal Article Meta-Analysis Review United States 2015/11/19 *Cardiovasc Eng Technol*. 2015 Jun;6(2):160-6. doi: 10.1007/s13239-015-0210-5. Epub 2015 Jan 21. 1
- [SWG05] SZPALA S., WIERZBICKI M., GUIRAUDON G., PETERS T. M.: Real-time fusion of endoscopic views with dynamic 3-d cardiac images: a phantom study. *IEEE Trans Med Imaging* 24, 9 (2005), 1207–15. Szpala, Stanislaw Wierzbicki, Marcin Guiraudon, Gerard Peters, Terry M Evaluation Study Journal Article Research Support, Non-U.S. Gov't Validation Study United States 2005/09/15 *IEEE Trans Med Imaging*. 2005 Sep;24(9):1207-15. doi: 10.1109/TMI.2005.853639. 1
- [YWA\*15] YANG L., WANG J., ANDO T., KUBOTA A., YAMASHITA H., SAKUMA I., CHIBA T., KOBAYASHI E.: Vision-based endoscope tracking for 3d ultrasound image-guided surgical navigation. *Computerized Medical Imaging and Graphics* 40 (2015), 205–216. 1